Journal of Sound and Vibration (2001) **247**(1), 131–144
doi:10.1006/jsvi.2001.3718, available online at http://www.idealibrary.com on IDEAL®

FREE FIELD VIBRATIONS DURING THE PASSAGE OF A THALYS HIGH-SPEED TRAIN AT VARIABLE SPEED

G. DEGRANDE

Department of Civil Engineering, K.U. Leuven, Kasteelpark Arenberg 40, *B*-3001 *Leuven, Belgium.*
E-mail: geert.degrande@bwk.kuleuven.ac.be

AND

L. SCHILLEMANS

Technum n.v., Interleuvenlaan 3, *B*-3001 *Leuven, Belgium*

(*Received* 24 *July* 2000, *and in final form* 12 *March* 2001)

During homologation tests of the high-speed train (HST) track between Brussels and Paris, free field vibrations and track response have been measured during the passage of a Thalys HST at speeds varying between 223 and 314 km/h. These experimental data are complementary to the other, but scarce, data sets published in the literature. Apart from illustrating the physical phenomena involved, this data set can be used for the validation of numerical prediction models for train-induced vibrations.

1. INTRODUCTION

Vibrations caused by the passage of a high-speed train (HST) are an environmental concern, as waves propagate through the soil and interact with nearby buildings, where they may cause malfunctioning of sensitive equipment and discomfort to people. The rapid extension of the high-speed rail network throughout Europe has initiated a lot of research on prediction models for train-induced vibrations. Analytical models [1–5] and numerical models using the finite and boundary element method [6–11] are under development to predict wave propagation and dynamic soil–structure interaction (SSI) due to the passage of a train. The models mainly differ in two aspects: the excitation mechanisms that are incorporated (quasi-static axle loads, parametric excitation, transient excitation due to rail joints and wheelflats and excitation due to wheel and rail roughness) and the way dynamic SSI is accounted for (through-soil coupling of the sleepers and the ballast). Track stability and vibrations generated at trans-Rayleigh train speeds for trains running on soft soils are subjects of particular interest.

Experimental data are needed for the validation of these numerical models. Available data sets are scarce, especially regarding the influence of the train speed on the vibration amplitudes. This is due to the fact that trains run at almost constant speed (e.g., 300 km/h on the HST Brussels–Paris track) once the track is in commercial operation.

Six weeks before the inauguration of the HST track between Brussels and Paris in December 1997, the Belgian railway company organized homologation tests during the passage of a Thalys HST at speeds varying between 160 and 330 km/h. This unique opportunity was taken to perform free field vibration measurements on the track and in the free field at distances varying from 4 to 72 m [12, 13]. The *in situ* measurements were

0022-460X/01/410131 + 14 $35.00/0

performed near Ath, 55 km south of Brussels, where the train can reach maximum speed. The results obtained are complementary to *in situ* vibration measurements performed during the passage of the Thalys HST on the Amsterdam–Utrecht track in the Netherlands at speeds between 40 and 160 km/h [14], to the data reported by Auersch [15] for the German ICE train at speeds varying between 100 and 300 km/h and to the measurements with the X2000 train on the West Coast Line in Sweden [16].

The objective of this paper is to make available this data set to other researchers so that it can be used for validation purposes. First, the characteristics of the Thalys HST and the track, as well as the dynamic soil characteristics are described. Second, the experimental set-up and the recorded passages are documented. Third, the time history and the frequency content of the vertical response of the rail, the sleeper and the free field at various distances to the track are discussed in detail for a single passage of the Thalys HST at a speed $v = 314$ km/h. Special attention is given, subsequently, to the influence of the train speed on the peak particle velocity (PPV) and the frequency content of the response in the free field. Validation of numerical models is beyond the scope of the present paper; we therefore refer to related papers [17, 18] where the present data set has been used to validate Krylov's analytical prediction model.

2. THE CHARACTERISTICS OF THE TRAIN, TRACK AND SOIL

2.1. THE CHARACTERISTICS OF THE THALYS HST

Figure 1 shows the configuration of the Thalys HST, consisting of two locomotives and eight carriages; the total length of the train is 200·18 m. The locomotives are supported by two bogies and have four axles. The carriages next to the locomotives share one bogie with the neighbouring carriage, while the six other carriages share both bogies with neighbouring carriages. The total number of bogies totals 13 and, consequently, the number of axles on the train is 26. The carriage length L_t, the distance L_b between bogies, the axle distance L_a, the total axle mass M_t, the sprung axle mass M_s and the unsprung axle mass M_u of all the carriages are summarized in Table 1.

2.2. THE CHARACTERISTICS OF THE TRACK

The HST track between Brussels and Paris is a classical ballast track (Figure 2). Continuously welded UIC 60 rails with a mass per unit length of 60 kg/m and a moment of inertia $I = 0{\cdot}3038 \times 10^{-4}\,\mathrm{m}^4$ are fixed with a Pandroll E2039 rail fixing system on precast, prestressed concrete monoblock sleepers of length $l = 2{\cdot}5$ m, width $b = 0.285$ m, height $h = 0{\cdot}205$ m (under the rail) and mass 300 kg. Flexible rail pads with thickness $t = 0{\cdot}01$ m and a static stiffness of about 100 MN/m, for a load varying between 15 and 90 kN, are placed under the rail. The track is supported by a porphyry ballast layer (calibre 25/50, layer

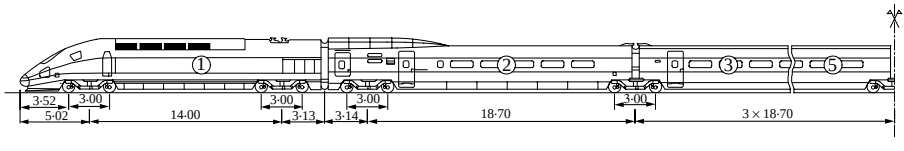

Figure 1. Configuration of the Thalys HST.

TABLE 1

Geometrical and mass characteristics of the Thalys HST

	Locomotives (2)	Outer carriages (2)	Central carriages (6)
axles/vehicle	4	3	2
L_t (m)	22·15	21·84	18·70
L_b (m)	14·00	18·70	18·70
L_a (m)	3·00	3·00	3·00
M_t (kg)	17 000	14 500	17 000
M_s (kg)	15 267	12 674	15 170
M_u (kg)	1733	1830	1826

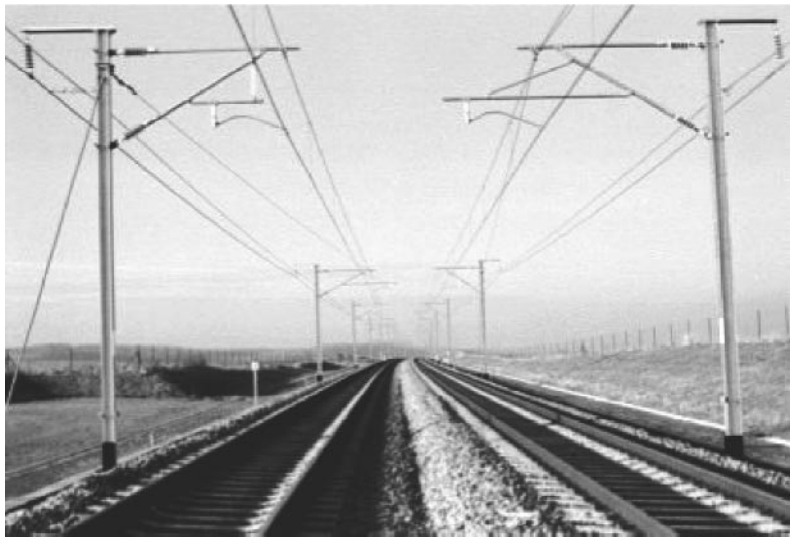

Figure 2. The HST track between Brussels and Paris.

thickness $d = 0{\cdot}3$ m), a limestone or porphyry layer (0/32, $d = 0{\cdot}2$ m) and a limestone supporting layer (0/80–0/120, $d = 0{\cdot}5$–$0{\cdot}7$ m).

During the homologation tests, access to the track was limited to the time needed for the installation of the accelerometers on the rails and the sleepers. No forced vibration test on the track could be performed to measure the frequency-dependent dynamic impedance of the track.

2.3. THE DYNAMIC SOIL CHARACTERISTICS

During the homologation tests, geophysical prospection tests have been performed. Due to time and budget limitations, non-intrusive geophysical prospection methods have been preferred, allowing for an estimate of the variation of the dynamic stiffness in the top layers and of a material damping ratio for an "equivalent" homogeneous half-space that exhibits similar attenuation at the surface as the test site.

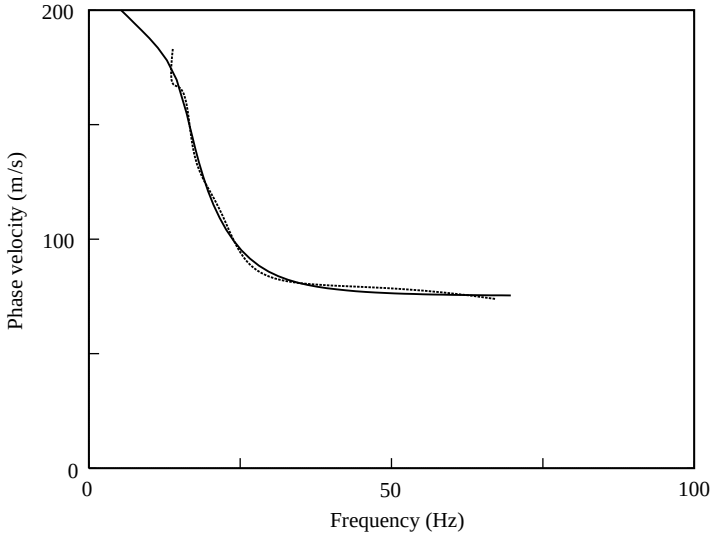

Figure 3. Comparison of the experimental (- - -) and theoretical (——) dispersion curve from the SASW test.

A spectral analysis of surface waves (SASW) has been performed to determine the dynamic soil characteristics of the site [19]. A transient excitation was generated by dropping a mass of 110 kg from a height of 0·9 m on a square (0·7 m × 0·7 m) steel foundation with a mass of 600 kg. A dashpot was used to control the frequency content of the loading and to prevent rebound of the mass. The vertical response was measured at 10 points on the surface at distances from 2 to 48 m from the source.

The inversion procedure minimizes the difference between the experimental and theoretical dispersion curve of the first surface wave, as illustrated in Figure 3. The latter corresponds to a horizontally stratified half-space with a top layer, with thickness $d = 1{\cdot}4$ m and a shear wave velocity $C_s = 80{\cdot}0$ m/s and a layer ($d = 1{\cdot}9$ m, $C_s = 133{\cdot}0$ m/s) on top of a half-space ($C_s = 226{\cdot}0$ m/s), in good agreement with the layering revealed by the borehole experiments. The track is constructed by excavation to a depth of a few meters, and stabilizing the soil under the ballast. As the SASW test was performed on the unexcavated soil away from the track, one may assume that the soil under the track is stiffer than the soft shallow layer revealed by the SASW test.

Apart from the variation of the stiffness with depth, an estimate of the hysteretic material damping is needed. As the cone penetration tests and the SASW test have revealed that the site is not homogeneous, the material damping ratio β^s is expected to vary with depth (it usually decreases with depth). In the following, however, the classical Barkan expression for a homogeneous half-space is used. This expression relates the vertical velocity $\hat{v}_z(r, \omega)$ at a distance r from the source to the vertical velocity $\hat{v}_z(r_1, \omega)$ at a reference distance r_1,

$$\hat{v}_z(r, \omega) = \hat{v}_z(r_1, \omega)[r/r_1]^{-n} \exp[-(2\pi\beta^s/\lambda_R)(r - r_1)], \tag{1}$$

where the exponent n represents the radiation damping in the soil and the coefficient β^s is the hysteretic material damping ratio. λ_R is the wavelength of the Rayleigh wave in the half-space. A simple inversion problem is obtained, from which a material damping ratio β^s can be derived for an equivalent homogeneous half-space, that exhibits similar attenuation at the surface as the test site.

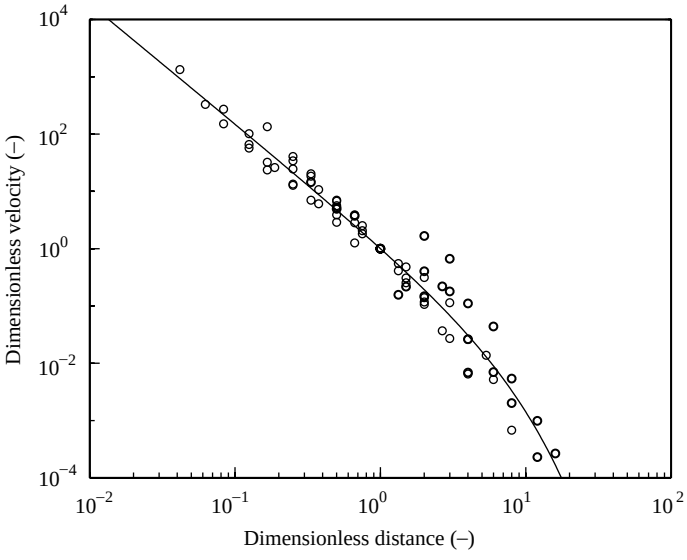

Figure 4. Dimensionless representation of the amplitude decay in the free field.

Figure 4 shows the dimensionless vertical velocity $\hat{v}_z(r,\omega)/\hat{v}_z(r_1,\omega)$ as a function of the dimensionless distance r/r_1, derived from the frequency content of the transient signals during the SASW test. The average Rayleigh wave velocity in the equivalent homogeneous half-space is taken as 80 m/s, the high-frequency limit of the first surface mode. A least-squares fit of these data reveals a radiation damping coefficient $n = 2{\cdot}10$ and a material damping ratio $\beta^s = 0{\cdot}03$. The estimated contribution of body waves is relatively high as the radiation damping coefficient n is closer to the theoretical value $n = 2$ for body waves and much higher than the theoretical value $n = 0{\cdot}5$ that prevails when surface waves dominate the response. In practice, material damping ratios are expected to decrease with depth and may be lower than the proposed value for deeper layers.

3. THE *IN SITU* EXPERIMENT

3.1. THE EXPERIMENTAL SET-UP

Vertical accelerations have been measured at 14 locations (Figure 5). On both tracks, a Dytran piezoelectric accelerometer was glued to the rail and the sleeper (Figure 6). In the free field, 10 seismic piezoelectric PCB accelerometers were placed at distances 4, 6, 8, 12, 16, 24, 32, 40, 56 and 72 m from the centre of track 2. They were mounted on steel or aluminium stakes with a cruciform cross-section to minimize dynamic soil–structure interaction effects (Figure 7).

A Kemo VBF 35 system was used as a power supply, amplifier and anti-aliasing filter with a low-pass frequency fixed at 500 Hz for the measurements on the track and 250 Hz in the free field. The signals were recorded with an analog 14-channel TEAC tape recorder. The A/D conversion was performed using a 16-bit Daqbook 216 data acquisition system at a sampling rate of 1000 Hz.

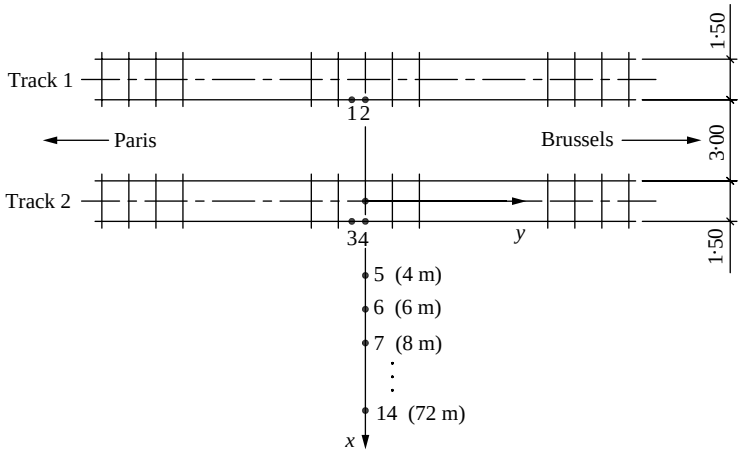

Figure 5. Location of the measurement points.

Figure 6. Accelerometers glued to the rail and sleeper of track 2.

3.2. THE RECORDED PASSAGES

Nine train passages at speeds varying between 223 and 314 km/h have been recorded, as summarized in Table 2. Each passage is labelled as *tij*, where *i* refers to the number of the

Figure 7. Seismic accelerometer mounted on an aluminium stake.

TABLE 2

Overview of recorded Thalys HST passages

Event	Track	Direction[+]	Speed (km/h)	Date	Passage
*t*11	1	P–B	223	3/11/97	4
*t*12	1	B–P	265	4/11/97	3
*t*13	1	P–B	272	3/11/97	6
*t*14	1	P–B	302	4/11/97	4
*t*21	2	B–P	256	3/11/97	5
*t*22	2	P–B	271	4/11/97	2
*t*23	2	B–P	289	4/11/97	1
*t*24	2	P–B	300	4/11/97	6
*t*25	2	B–P	314	4/11/97	5

[+] P—Paris; B—Brussels.

track and *j* numbers the event; the passages on each track are ordered according to the increasing train speed. Measurements have been made in a wide range of train speeds compared to the commercial operating speed of the Thalys HST at this location, which is 300 km/h.

Figure 8. Passage of the Thalys HST on track 2 with a speed $v = 314\,\text{km/h}$.

As an example, the track and free field response during the passage of the Thalys HST on track 2 with a speed $v = 314\,\text{km/h}$ (Figure 8) will be discussed in detail in the following section. Results for other train speeds are summarized in a subsequent section, so that conclusions can be drawn regarding the influence of the train speed on the PPV and frequency content of the response. Whereas the raw data have been measured in a reference frame with the z-axis pointing upwards, it is more usual in soil dynamics to choose the co-ordinate frame of reference with the z-axis pointing downwards. The latter convention is used in all figures.

4. THE PASSAGE OF A THALYS HST AT A SPEED OF 314 km/h

4.1. TRACK RESPONSE

Figure 9 shows the time history and frequency content of the vertical acceleration of the rail and the sleeper during the passage of the Thalys HST on track 2 with a speed $v = 314\,\text{km/h}$.

Very high accelerations upto $250\,\text{m/s}^2$ are observed on the rail (Figure 9(a)). The passage of individual bogies and axles can clearly be noticed in the acceleration time history. The time separation between the passage of the bogies 2 and 3, and 11 and 12 is small, however. The frequency content of the acceleration response is very broad (Figure 9(b)).

The acceleration time history of the sleeper (Figure 9(c)) shows much lower amplitudes than for the rail. It clearly allows the identification of the passage of all individual axles. The acceleration has a quasi-discrete spectrum (Figure 9(d)) with peaks at the fundamental bogie passage frequency $f_b = v/L_b = 4{\cdot}66\,\text{Hz}$ and its higher order harmonics, modulated at the axle passage frequency $f_a = v/L_a = 29{\cdot}07\,\text{Hz}$. This spectrum corresponds qualitatively with the spectrum of the sleeper displacement during the passage of a train when the track is modelled as a beam on elastic foundation [5].

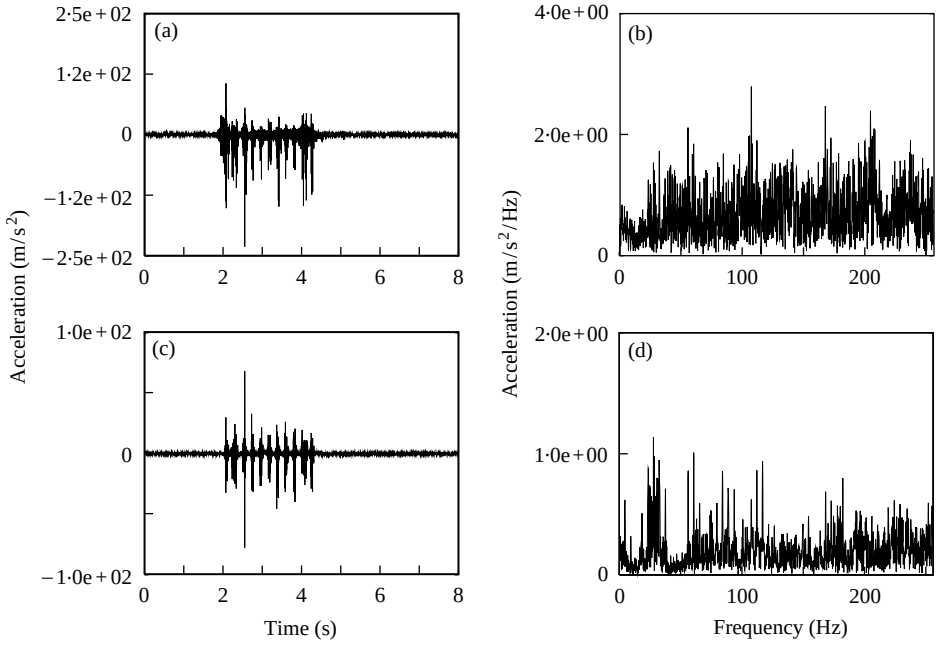

Figure 9. Measured time history (left) and frequency content (right) of the vertical acceleration of the rail and the sleeper during the passage of the Thalys HST on track 2 with a speed $v = 314$ km/h. (a) a_z (*Rail*, t); (b) $\hat{a}_z$ (*Rail*, ω); (c) a_z (*Sleeper*, t); (d) $\hat{a}_z$ (*Sleeper*, ω).

4.2. FREE FIELD RESPONSE

Figures 10 and 11 summarize the time history and frequency content of the vertical velocity of the rail, the sleeper, and the soil at all distances from the centre of track 2. Velocities are obtained by integration of the accelerations, after the removal of electrical noise; a digital filter with $N = 500$ weighting functions, a roll-off termination frequency $f_t = 2{\cdot}5$ Hz and a cut-off frequency $f_c = 3{\cdot}0$ Hz is used to eliminate the DC component and avoid drifting [20]. In Figures 10 and 11, the vertical scale is kept constant for those channels where the same type of accelerometer has been used, so that the effect of radiation and material damping in the soil on the amplitudes for increasing distance and excitation frequency can be better appreciated.

In the near field, the time history of the vertical response $v_z(x^R = 6, t)$ at 6 m from the track is considered. Figure 10(d) enables the identification of the passage of the individual bogies, whereas the passage of the axles can no longer be distinguished. The PPV is about 2·5 mm/s. Due to the specific train composition, the observed velocity spectrum $\hat{v}_z(x^R = 6, \omega)$ (Figure 11(d)) is quasi-discrete with a maximum at the fundamental bogie passage frequency $f_b = 4{\cdot}66$ Hz. The sleeper passage frequency $f_s = v/d = 145{\cdot}37$ Hz, with $d = 0{\cdot}6$ m the sleeper distance, is still noticeable in the spectrum. Similar observations can be made regarding the response in other nearfield receivers.

Next, the response in the far field at a larger distance from the track, at 40 m for example, is considered, which allows to observe the effect of radiation and material damping in the soil. The time history $v_z(x^R = 40, t)$ (Figure 10(j)) shows a PPV of about 0·2 mm/s. Notice the improvement of the signal-to-noise ratio between the signal recorded at 40 m from the track with respect to the signal at 32 m; this is due to the use of accelerometers with a sensitivity that is 10 times higher (10 V/g instead of 1 V/g) for distances higher than 32 m.

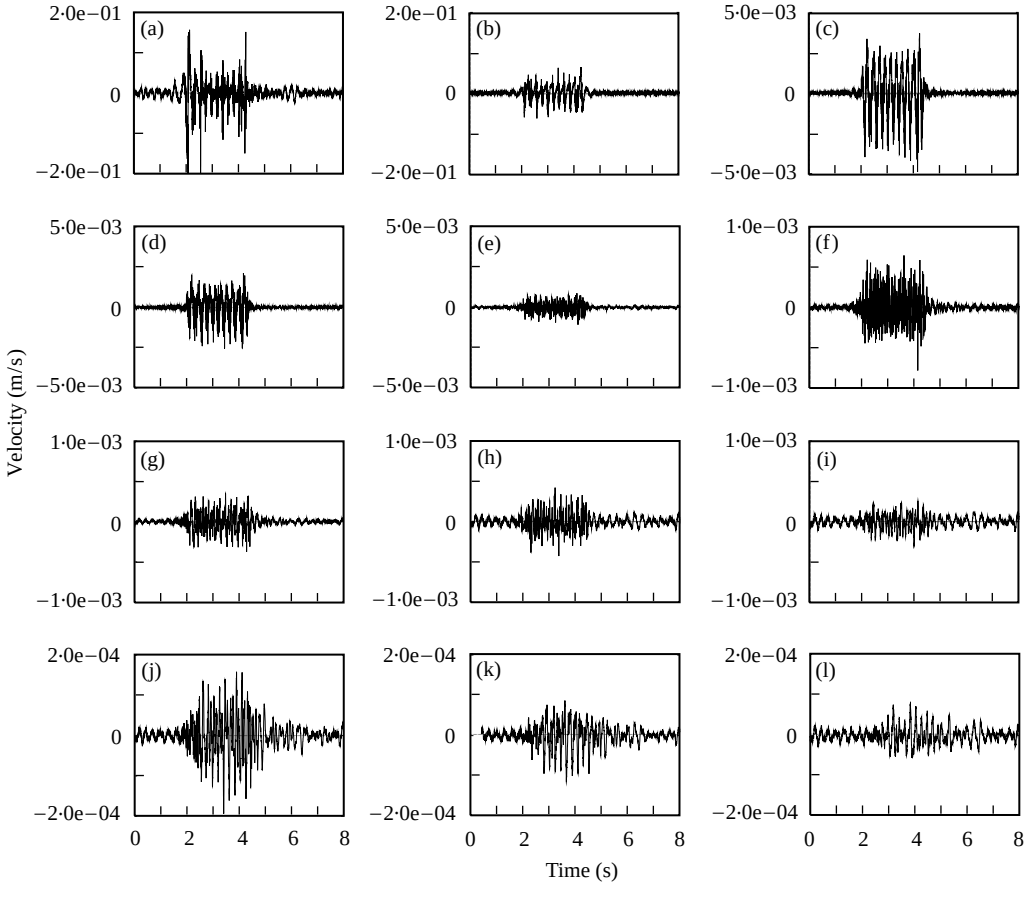

Figure 10. Measured time history of the vertical velocity on the track and in the free field for the passage of the Thalys HST on track 2 with $v = 314$ km/h: (a) v_z (*Rail*, t); (b) v_z (*Sleeper*, t); (c) v_z ($x^R = 4, t$); (d) v_z ($x^R = 6$, t); (e) $v_z(x^R = 8, t)$; (f) $v_z(x^R = 12, t)$; (g) $v_z(x^R = 16, t)$; (h) $v_z(x^R = 24, t)$; (i) $v_z(x^R = 32, t)$; (j) $v_z(x^R = 40, t)$; (k) $v_z(x^R = 56, t)$; (l) v_z ($x^R = 72$, t).

The velocity spectrum $\hat{v}_z(x^R = 40, \omega)$ (Figure 11(j)) is dominated by the bogie passage frequency and its second harmonic. Higher frequencies are attenuated by radiation and material damping in the soil. The sleeper passage frequency, for example, can no longer be observed.

5. THE INFLUENCE OF THE TRAIN SPEED

An important question is how the train speed affects the time history and frequency content of the free field response at various distances from the track.

As an example, Figure 12 shows the time history and frequency content of the vertical velocity at 8 m from track 2 during the passage of a Thalys HST on track 2 at five different train speeds, varying from 256 to 314 km/h. Although the duration of the signal is evidently affected by the train speed, the time histories do not show a strong dependency of the PPV on the train speed. The shift of the spectra towards higher frequencies for increasing train

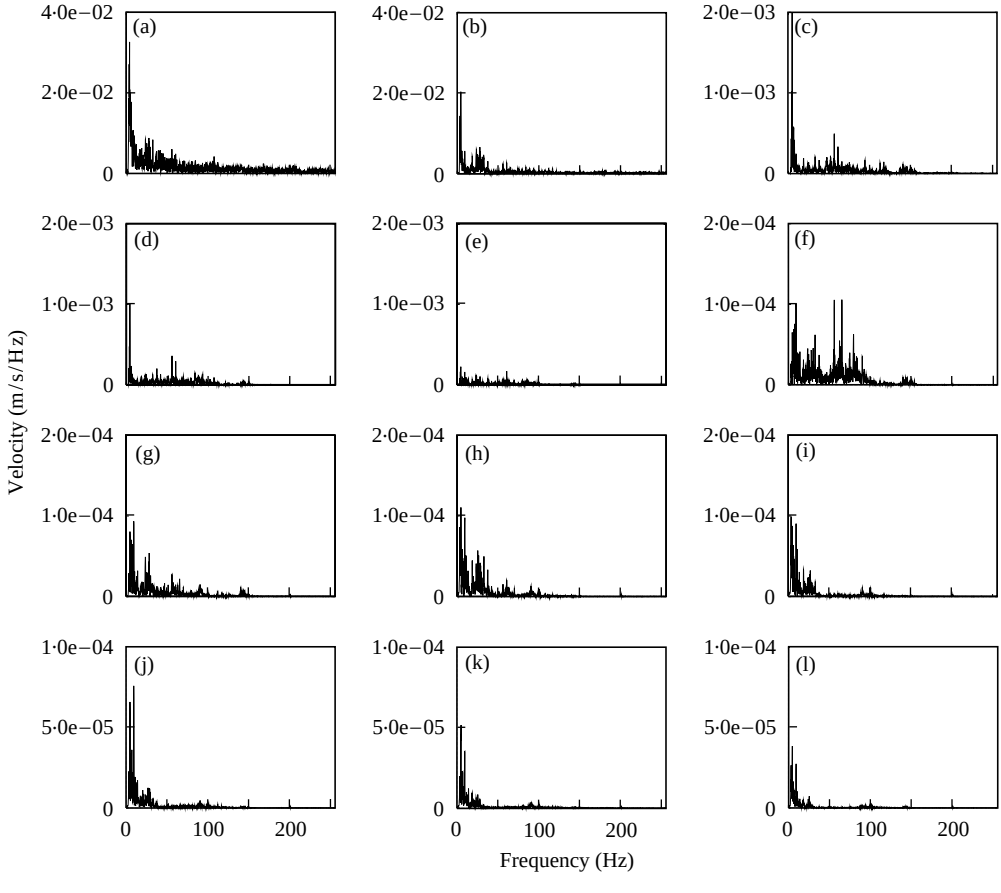

Figure 11. Measured frequency content of the vertical velocity on the track and in the free field for the passage of the Thalys HST on track 2 with $v = 314$ km/h: (a) $\hat{v}_z$ (*Rail*, ω); (b) $\hat{v}_z$ (*Sleeper*, ω); (c) $\hat{v}_z$ ($x^R = 4, \omega$); (d) $\hat{v}_z$ ($x^R = 6, \omega$); (e) $\hat{v}_z(x^R = 8, \omega)$; (f) $\hat{v}_z(x^R = 12, \omega)$; (g) $\hat{v}_z(x^R = 16, \omega)$; (h) $\hat{v}_z(x^R = 24, \omega)$; (i) $\hat{v}_z(x^R = 32, \omega)$; (j) $\hat{v}_z(x^R = 40, \omega)$; (k) $\hat{v}_z(x^R = 56, \omega)$; (l) $\hat{v}_z$ ($x^R = 72$, ω).

speed is especially clear when the sleeper passage frequency is considered: the latter varies from 118·52 Hz at a speed $v = 256$ km/h to 145·37 Hz at a speed $v = 314$ km/h.

The previous observations, based on the response at a single receiver at 8 m from track 2, are confirmed in Figure 13 where the PPV is shown as a function of the receiver distance to the track for Thalys HST passages on tracks 1 and 2 at different speeds. The decrease of PPV with distance due to radiation and material damping in the soil can clearly be observed. Figure 13 shows only a very moderate tendency of increasing vibration levels for increasing train speed. The same conclusion can be drawn from Figure 14, where the PPV is shown as a function of the train speed for all distances to the track.

6. CONCLUSION

The results of free field vibration measurements during the passage of a Thalys HST at a speed varying between 223 and 314 km/h on the new HST track between Brussels and Paris have been presented. These experimental data are complementary to other data sets

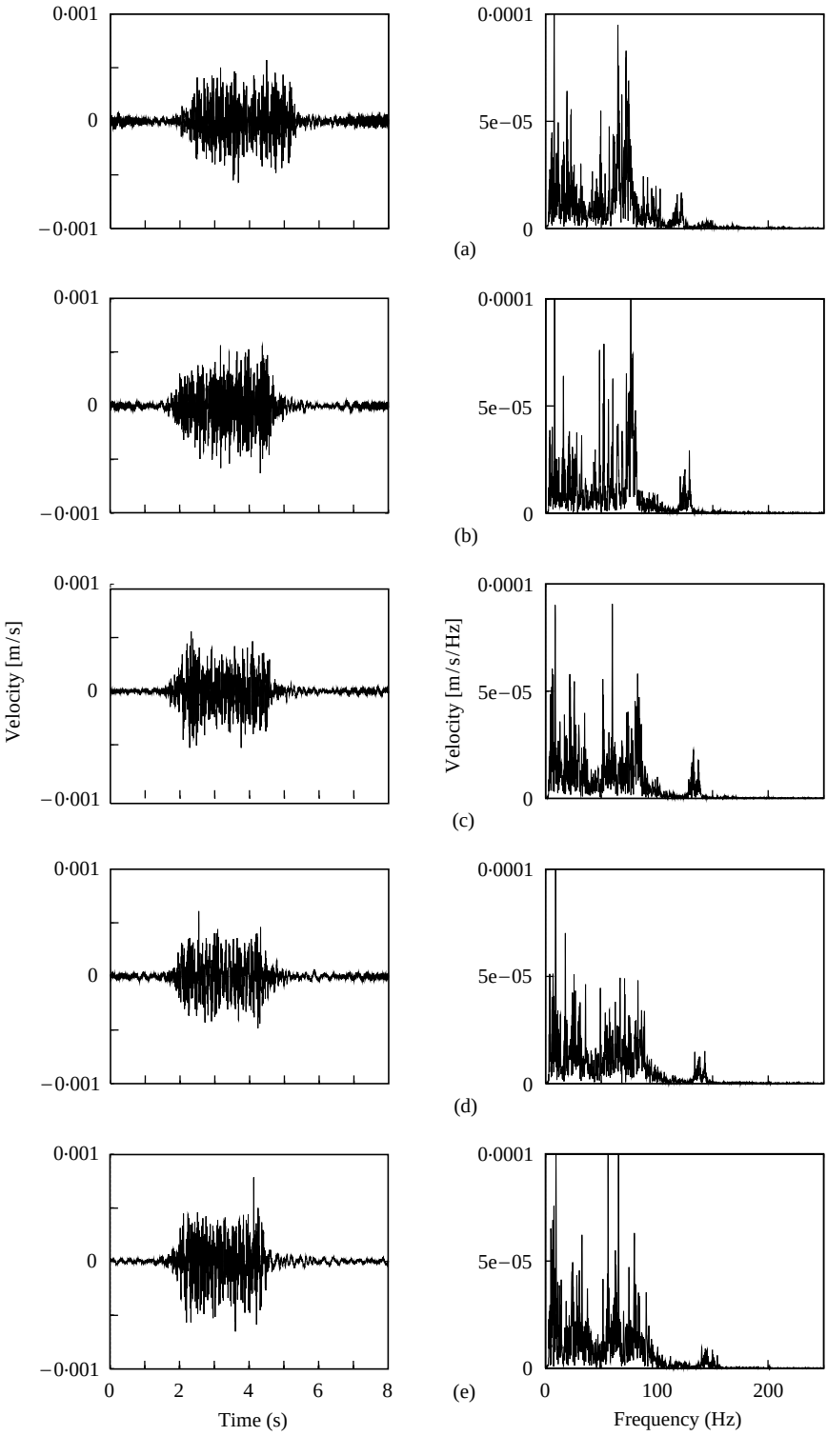

Figure 12. Measured time history (left) and frequency content (right) of the vertical velocity at 8 m from track 2 during the passage of a Thalys HST on track 2 at varying speeds (km/h): (a) 256; (b) 271; (c) 289; (d) 300; (e) 314.

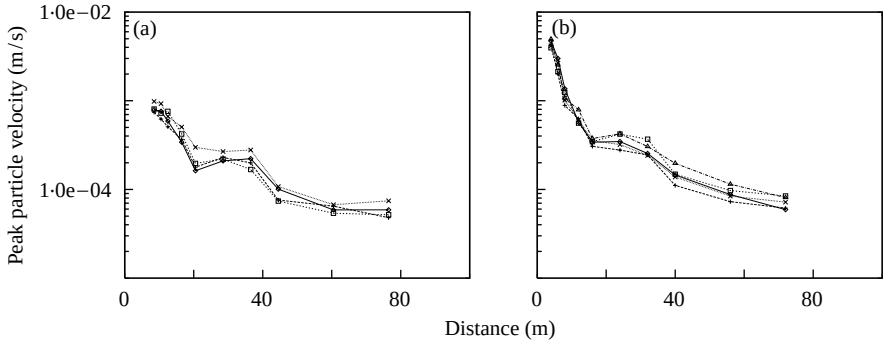

Figure 13. Measured PPV as a function of the distance to the track for different train speeds (km/h) for Thalys HST passages on (a) track 1: —◇—, 223; -- + --, 265; ···□···, 272; — × —, 302; (b) track 2: —◇—, 256; -- + --, 271; ···□···, 289; ··· × ···, 300; − · −△− · −, 314.

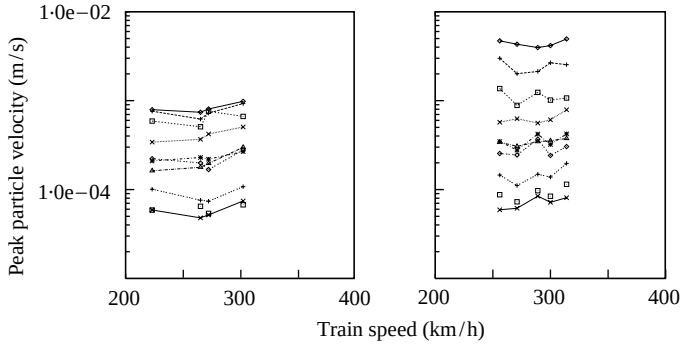

Figure 14. Measured PPV as a function of the train speed for different receiver distances (m) for Thalys HST passages on (a) track 1: —◇—, 8·5; -- + --, 10·5; ···□···, 12·5; ··· × ···, 16·5: —.—△—.—, 20·5; ···✱···, 28·5; − − −◇− − −, 36·5; -- + --, 44·5; − − −□− − −, 60·5; — × —, 76·5; (b) track 2: —◇—, 4·0; -- + --, 6·0; ···□···, 8·0; --- × ---, 12·0: − · −△− · −, 16·0; ···✱···, 24·0; ---◇---, 32·0; --- + ---, 40·0; ---□---, 56·0; — × —, 72·0.

published in the literature; the fact that measurements have been made at nine different train speeds makes this data set unique. Only a very weak dependence of the PPV on the train speed has been demonstrated.

Although time and budget constraints have limited the extent of the parameter identification, especially the dynamic impedance of the track and the variation with depth of the hysteretic material damping in the soil, we believe that this data set is useful to validate numerical prediction models for HST induced vibrations.

The interested reader is referred to our web site at `http://www.bwk.kuleuven.ac.be/bwm/` from where the data files can be downloaded.

ACKNOWLEDGMENTS

The *in situ* experiments have been performed with the assistance of K. Peeraer. The collaboration of P. Godart and W. Bontinck of the NMBS is kindly acknowledged. W. Dewulf has inverted the SASW data.

REFERENCES

1. H. GRUNDMANN, M. LIEB, and E. TROMMER 1999 *Archives of Applied Mechanics* **69**, 55–67. The response of a layered half-space to traffic loads moving along its surface.
2. H. E. M. HUNT 1996 *Journal of Sound and Vibration* **193**, 185–194. Modelling of rail vehicles and track for calculation of ground vibration transmission into buildings.
3. V. V. KRYLOV 1994 *Journal de Physique IV* **4**, 769–772. On the theory of railway-induced ground vibrations.
4. V. V. KRYLOV 1995 *Applied Acoustics* **44**, 149–164. Generation of ground vibrations by superfast trains.
5. V. V. KRYLOV 1998 *Acustica-Acta Acustica* **84**, 78–90. Effects of track properties on ground vibrations generated by high-speed trains.
6. A. M. KAYNIA, C. MADSHUS and P. ZACKRISSON 2000. *Journal of Geotechnical and Geoenvironmental Engineering, Proceedings of the American Society of Civil Engineers*, **126**, 531–537. Ground vibration from high speed trains: prediction and countermeasure.
7. K. KNOTHE and Y. WU 1998 *Archives of Applied Mechanics* **68**, 457–470. Receptance behaviour of railway track and subgrade.
8. W. RÜCKER 1981 *Forschungsbericht* 78, *Bundesanstalt für Materialforschung und-prüfung, Berlin*. Dynamische Wechselwirkung eines Schienen-Schwellensystems mit dem Untergrund.
9. X. SHENG, C. J. C. JONES and M. PETYT 1999 *Journal of Sound and Vibration* **225**, 3–28. Ground vibration generated by a harmonic load acting on a railway track.
10. X. SHENG, C. J. C. JONES and M. PETYT 1999 *Journal of Sound and Vibration* **228**, 129–156. Ground vibration generated by a load moving along a railway track.
11. P. VAN DEN BROECK and G. DE ROECK 1999 in *Proceedings of the 4th European Conference on Structural Dynamics: Eurodyn '99, Prague, Czech Republic, June* 7–10 (L. Frýba and J. Náprstek, editors), 837–842. Rotterdam: A. A. Balkema. The vertical receptance of track including soil–structure interaction.
12. G. DEGRANDE and L. SCHILLEMANS 1998 in *Proceedings ISMA* 23, *Noise and Vibration Engineering*, Vol. III, *Leuven, Belgium, September* (P. Sas, editor), 1563–1570. Free field vibrations during the passage of a HST.
13. G. DEGRANDE 2001 in *Noise and Vibration from High-speed Trains*, (V. V. Krylov, editor), 283–312. London: Thomas Telford Publishing. Free field vibrations during the passage of a high speed train: experimental results and numerical predictions.
14. J. BRANDERHORST 1997 *Master's Thesis, Universiteit Twente, Holland Railconsult*. Modellen voor het boeggolfprobleem bij hogesnelheidstreinen. Ontwerp en validatie met behulp van de resultaten van de proef Amsterdam–Utrecht.
15. L. AUERSCH 1989 *Forschungsbericht* 155, *Bundesanstalt für Materialforschung und—prüfung, Berlin*. Zur Entstehung und Ausbreitung von Schienenverkehrserschutterungen — theoretische Untersuchungen und Messungen an Hochgeschwindigkeitszug Intercity Experimental.
16. K. ADOLFSSON, B. ANDRÉASSON, P.-E. BENGTSON, A. BODARE, C. MADSHUS, R. MASSARCH, G. WALLMARK and P. ZACKRISSON 1999 *Technical Report, Banverket, Sweden*. High speed lines on soft ground. Evaluation and analyses of measurements from the West Coast Line.
17. G. DEGRANDE 1999 in *Proceedings of the 13th ASCE Engineering Mechanics Division Specialty Conference, Baltimore, MD, U.S.A., June* 13–16 (P. Jones and R.G. Ghanem, editors). CD-ROM. Free field vibrations during the passage of a high speed train: validation of a numerical model by means of experimental results.
18. G. LOMBAERT and G. DEGRANDE 2000 in *Proceedings of the 7th International Congress on Sound and Vibration, Garmisch-Partenkirchen, Germany, July* (G. Guidati, H. Hunt, H. Heller and A. Heiss, editors), 2671–2678. An efficient formulation of Krylov's prediction model for train induced vibrations based on the dynamic reciprocity theorem.
19. W. DEWULF, G. DEGRANDE and G. DE ROECK 1996 *Conference on Inverse Problems of Wave Propagation and Diffraction, Aix-les-Bains, France, September*. Spectral analysis of surface waves: an automated inversion technique based on a Gauss–Newton inversion algorithm.
20. J. F. A. ORMSBY 1961 *Journal of the Association for Computing Machinery* **8**, 440–466. Design of numerical filters with application to missile data processing.